



# Geostatistics in the Presence of Multivariate Complexities: Comparison of Multi-Gaussian Transforms

Sultan Abulkhair<sup>1,2</sup> · Peter A. Dowd<sup>1,2</sup> · Chaoshui Xu<sup>2</sup>

Received: 5 November 2022 / Accepted: 6 March 2023  
© The Author(s) 2023

## Abstract

One of the most challenging aspects of multivariate geostatistics is dealing with complex relationships between variables. Geostatistical co-simulation and spatial decorrelation methods, commonly used for modelling multiple variables, are ineffective in the presence of multivariate complexities. On the other hand, multi-Gaussian transforms are designed to deal with complex multivariate relationships, such as non-linearity, heteroscedasticity and geological constraints. These methods transform the variables into independent multi-Gaussian factors that can be individually simulated. This study compares the performance of the following multi-Gaussian transforms: rotation based iterative Gaussianisation, projection pursuit multivariate transform and flow transformation. Case studies with bivariate complexities are used to evaluate and compare the realisations of the transformed values. For this purpose, commonly used geostatistical validation metrics are applied, including multivariate normality tests, reproduction of bivariate relationships, and histogram and variogram validation. Based on most of the metrics, all three methods produced results of similar quality. The most obvious difference is the execution speed for forward and back transformation, for which flow transformation is much slower.

**Keywords** Rotation based iterative Gaussianisation · Projection pursuit multivariate transform · Flow transformation · Minimum/maximum autocorrelation factors · Complex bivariate relationships

---

✉ Sultan Abulkhair  
sultan.abulkhair@adelaide.edu.au

<sup>1</sup> ARC Training Centre for Integrated Operations for Complex Resources, University of Adelaide, Adelaide, Australia

<sup>2</sup> School of Civil, Environmental and Mining Engineering, University of Adelaide, Adelaide, Australia

## 1 Introduction

Geostatistical conditional simulation often requires the modelling of multiple cross-correlated variables. For example, multivariate geostatistics is commonly applied to model ore grades and other mineral deposit variables (Journel and Huijbregts 1978; Wackernagel 2003). Among the Gaussian methods, there are three ways to perform this task (Rossi and Deutsch 2014). The first is to use conditional co-simulation algorithms such as sequential Gaussian co-simulation (Verly 1993) and turning bands co-simulation (Emery 2008). The second approach is to use hierarchical co-simulation, which enables full, collocated and multi-collocated co-kriging to be applied (Almeida and Journel 1994). Finally, the third way is to transform variables into uncorrelated factors and simulate them individually.

Direct and hierarchical co-simulations use a linear model of co-regionalisation (LMC) (Journel and Huijbregts 1978) or a Markov model (Journel 1999) to account for cross-correlations between variables. However, inference of cross-variograms can be challenging, whereas transformation to independent factors significantly simplifies multivariate modelling. For example, principal component analysis (PCA) and independent component analysis (ICA) have been applied in geostatistics to transform cross-correlated variables into independent orthogonal factors (Davis and Greenes 1983; Tercan and Sohrabian 2013). However, the validity of extending PCA and ICA decorrelation to non-zero lag distances is an assumption. Alternatively, minimum/maximum autocorrelation factors (MAF) performs a double spectral decomposition at lag zero and a single non-zero lag to achieve spatial decorrelation (Desbarats and Dimitrakopoulos 2000). Other spatial decorrelation methods applied in geostatistics are uniformly weighted exhaustive diagonalisation with Gauss iterations and rotational joint diagonalisation (Mueller and Ferreira 2012; Mueller et al. 2020).

Geostatistical co-simulation is also limited by the multi-Gaussianity assumption, which is often unrealistic as there may be complex multivariate relationships (Barnett et al. 2014). LMC cannot include these complexities in a covariance matrix, and linear transformations (e.g., PCA, ICA and MAF) are only applicable to linear relationships. This motivated Leuangthong and Deutsch (2003) to apply stepwise conditional transformation (SCT) in the geostatistical framework to deal with multivariate complexities, such as non-linearity, heteroscedasticity and inequality constraints. In geostatistics, SCT was the earliest application of a multi-Gaussian transform (MGT). The idea behind MGT approaches is to simply transform variables into standard multivariate Gaussian distributions with zero correlation. SCT removes the complexities by transforming the original variables into multi-Gaussian factors. However, SCT cannot handle high-dimensional datasets and it requires extensive data cleaning and the order of the variables to be predefined (Rossi and Deutsch 2014). Recently, de Figueiredo et al. (2021) proposed a direct multivariate simulation based on SCT and demonstrated its applicability to a six-dimensional dataset with non-linear relationships.

Two of the most popular MGT methods in geostatistics are the projection pursuit multivariate transform (PPMT) (Barnett et al. 2014, 2016) and flow transformation, also known as flow anamorphosis (FA) (van den Boogaart et al. 2017). PPMT searches for the direction that has the maximum projection index (Friedman 1987) and applies a normal score transformation in that direction. It is an iterative algorithm that transforms

the data along projections based on the departure from Gaussianity. PPMT can be applied to a higher number of variables than SCT, it can work with smaller datasets and does not need the order of variables to be predefined (Barnett et al. 2014). On the other hand, FA continuously deforms the original distribution into multi-Gaussian space using Lagrangian mechanics (van den Boogaart et al. 2017). Furthermore, its affine equivariance makes FA suitable for compositional data analysis (Tolosana-Delgado et al. 2019), in which it can be paired with various log-ratio transforms (Pawlowsky-Glahn et al. 2015).

A case study of the Gol-e-Gohar iron deposit by Hosseini and Asghari (2019) suggests that the combination of log-ratio+FA+MAF produces fewer artefacts during back transformations and provides better reproduction of compositional constraints than the combination of PPMT+MAF. In the case study, the additive log-ratio transformation was chained only with FA because of its affine equivariance. However, Manchuk et al. (2017) successfully chained PPMT with an isometric log-ratio transformation (Egozcue et al. 2003) to reproduce the sum constraint. Similarly, additive and fraction ratios (i.e., not logarithmic) have been used on PPMT factors to reproduce sum and fractional constraints, also known as inequality constraints (Bassani et al. 2018). Nevertheless, it is also essential to chain these methods with MAF or any other spatial decorrelation to ensure that factors are independent at non-zero lags. For example, the combination of PPMT+MAF shows significantly better variogram reproduction compared to the transformation by PPMT or by MAF (Erten and Deutsch 2021).

This study compared the performance of PPMT, FA and a relatively new method to geostatistics, rotation based iterative Gaussianisation (RBIG) (Laparra et al. 2011). RBIG is similar to PPMT, but it rotates the data using either PCA or ICA and applies the normal score transformation after each rotation. The following sections provide more details on selected methods together with a comprehensive comparison based on different metrics. The comparison is based on three bivariate case studies from undisclosed mining deposits with strong multivariate complexities. The results were carefully assessed using different statistical and qualitative metrics.

## 2 Materials and Methods

### 2.1 Case Studies with Multivariate Complexities

This paper applies selected methods to three bivariate case studies with complex relationships (Fig. 1). These are confidential mining datasets and are, therefore, undisclosed. Case A consists of 6074 drill hole samples for which there is an inequality constraint between total and soluble copper grades. The average horizontal spacing between samples is 123 m with a composite length of 2 m. This type of multivariate complexity occurs when one variable is a fraction of another variable, and there have been attempts to model this relationship (Hosseini and Asghari 2015; Bassani et al. 2018; Abildin et al. 2019). Inequality constraints can also occur in iron ore deposits between iron and elements such as silica and aluminium oxide when there is a linear inequality between variables (Madani and Abulkhair 2020; Abulkhair and Madani 2021).

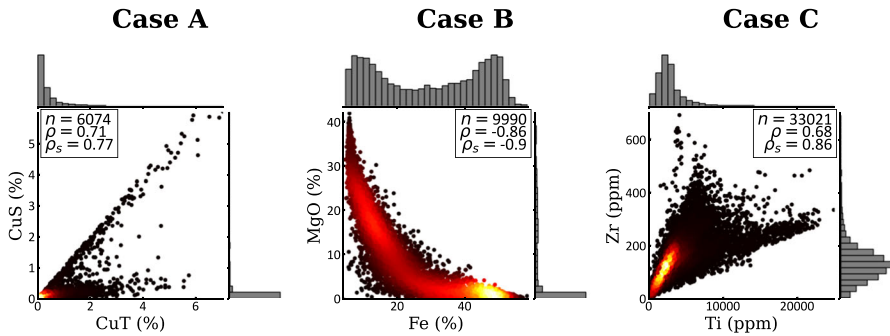


**Fig. 1** Cross plots of three bivariate case studies with an inequality constraint (case A), non-linearity (case B) and heteroscedasticity (case C). Number of samples, Pearson  $\rho$  and Spearman  $\rho_s$  correlation coefficients are shown in text boxes

For case B, there is a non-linearity between 9,990 iron and magnesium oxide samples. In this case, the sample points are irregularly spaced with an average of 4.2 m for horizontal and 2.4 m for vertical spacing. Non-linearities are not rare in drill hole datasets, and several geostatistical case studies have focussed on modelling such datasets (Leuangthong and Deutsch 2003; Barnett et al. 2014, 2016; de Figueiredo et al. 2021; Erten and Deutsch 2021).

Finally, the case C data come from an underground mine with an average of 14.5 m spacing and a composite length of 2 m. It is a bivariate dataset with 33,021 samples of titanium and zirconium with a heteroscedastic relationship between them. Heteroscedasticity is similar to a linear relationship, expressed by a non-constant variance of one variable across the range of values of another. Heteroscedastic relationships has been reported in many multivariate geostatistical studies (Barnett et al. 2014, 2016; de Figueiredo et al. 2021; Erten and Deutsch 2021). However, case C demonstrates a more obvious heteroscedastic relationship with a moderately high correlation.

As all three cases are mining datasets prone to sampling irregularities, duplicates and outliers, they underwent careful data cleaning. In addition, cell declustering (Deutsch and Journel 1992) was applied for cases A and B. Cells of  $85\text{ m} \times 85\text{ m} \times 85\text{ m}$  were chosen for case A and  $18\text{ m} \times 18\text{ m} \times 18\text{ m}$  for case B after evaluating the effect of different cell sizes. As a result, mean and standard deviation values decreased after declustering for both cases. Cell declustering was not performed for case C because the sum of weights was not equal to the number of samples. Table 1 shows the descriptive statistics for all three case studies. As multivariate complexities are involved, both Spearman and Pearson correlation coefficients are reported.

## 2.2 Multivariate Transformation

### 2.2.1 Rotation Based Iterative Gaussianisation

RBIG is an iterative algorithm that applies marginal Gaussianisation followed by an orthonormal rotation. Although Laparra et al. (2011) demonstrated that any orthonormal rotation, even a simple random rotation matrix, could be used in RBIG, PCA and

**Table 1** Descriptive statistics of three bivariate datasets

Parameter	Case A		Case B		Case B	
	CuT (%)	CuS (%)	Fe (%)	MgO (%)	Ti (ppm)	Zr (ppm)
Mean	0.42	0.12	29.01	8.86	2928.88	128.75
Standard deviation	0.64	0.39	16.10	10.60	2357.84	64.01
Pearson correlation	0.71		-0.86		0.68	
Spearman correlation	0.77		-0.90		0.86	

ICA are more suitable. The choice of a rotation matrix is important and is usually based on multiple factors. PCA provides a suboptimal convergence rate compared to ICA and requires more iterations. However, convergence in ICA takes more time, especially in higher dimensional cases. In this study, we used RBIG with both PCA (RBIGP) and ICA (RBIGI) rotations for comparison. For RBIGP, the original MATLAB code from Laparra et al. (2011) was implemented with histogram equalisation for marginal Gaussianisation. For RBIGI, a Python implementation was used with a normal score transformation for marginal Gaussianisation together with fast ICA (Hyvarinen 1999) from the Scikit-learn library (Pedregosa et al. 2011) for rotation.

The steps in RBIG are as follows:

1. First marginal Gaussianisation

$$Y_{(0)} = \Psi_{(0)}(Z), \quad (1)$$

where  $\Psi_{(0)}(Z)$  is a normal score transformation for RBIGI or histogram equalisation for RBIGP applied to each dimension of the original data  $Z$  before the first iteration.

2. ICA or PCA rotation expressed by an orthonormal rotation matrix  $R_{(i)}$  at each iteration  $i$

$$Y_{(i+1)}^{\text{Rot}} = R_{(i)} Y_{(i)}^{\text{Gaus}}. \quad (2)$$

3. Marginal Gaussianisation of rotated variables at each iteration  $i$

$$Y_{(i+1)}^{\text{Gaus}} = \Psi_{(i)}(Y_{(i+1)}^{\text{Rot}}). \quad (3)$$

4. Repeat steps 2 and 3 for a predefined number of iterations.

In this study, the algorithm runs for a fixed number of iterations without any stopping criteria. In addition, RBIG saves rotation matrices and Gaussian tables at each iteration, including the first marginal Gaussianisation. Finally, the back transformation to the original state is performed in reverse order of the data saved at each iteration.

## 2.2.2 Projection Pursuit Multivariate Transform

PPMT methodology is based on iteratively searching for interesting projections followed by normal score transformation along those projections (Barnett et al. 2014, 2016). An interesting projection is one that has a maximum departure from Gaussianity based on the projection index developed by Friedman (1987). The input parameters for the original algorithm are a maximum number of iterations and stopping criteria. The algorithm terminates after reaching the targeted projection index percentile based on the bootstrapping algorithm or after a set number of iterations (Barnett et al. 2014). A detailed description and visualization of PPMT and its stopping criteria can be found in Barnett et al. (2016).

Similar to RBIG, PPMT runs for a fixed number of iterations in this study. The purpose of doing so is to check the multivariate normality of the transformed RBIG and PPMT factors after the same number of iterations. PPMT records rotation matrices and Gaussian tables at each step, which are used during the back transformation following the above steps in reverse order. We used a Python implementation of PPMT based on the original Fortran code from Barnett et al. (2014).

## 2.2.3 Flow Transformation

The FA methodology differs from that of RBIG and PPMT, which are based on orthonormal rotations and marginal Gaussianisations. FA continuously deforms the original kernel density function into standard multi-Gaussian space using Lagrangian mechanics (van den Boogaart et al. 2017). The two main input parameters that characterise this deformation are the starting  $\sigma_0$  and the final  $\sigma_1$  spreads of the kernel that control the smoothing. This means that  $\sigma_0$  controls how strongly FA deforms the kernels, for which a smaller value results in more Gaussian factors. In contrast,  $\sigma_1$  controls the ranges of the produced factors, and it is recommended that  $\sigma_1 = \sigma_0 + 1$  so that the marginal distributions of the transformed data have standard deviations close to 1 (Talebi et al. 2019). For the details of the methodology of the FA algorithm, readers are referred to the original literature (van den Boogaart et al. 2017; Tolosana-Delgado and Mueller 2021).

In this study, the “gmGeostats” CRAN package (Tolosana-Delgado and Mueller 2021) was used for FA and the transformation was chained twice to achieve multivariate normality.

## 2.2.4 Chained Multi-Gaussian Transform and Spatial Decorrelation

MGT methods, similar to PCA and ICA linear transforms, can only guarantee a decorrelation at lag zero. A practical solution to ensure spatial decorrelation is to chain those methods with MAF (Desbarats and Dimitrakopoulos 2000). The original geostatistical application of MAF uses PCA twice, once on a covariance matrix at lag 0 and once on a single non-zero lag of the cross-variogram function. However, as RBIG, PPMT or FA already produce independent factors, only the second MAF is used. Chained MGT and MAF comprise the following steps:

1. Transform the original data  $Z$  into independent standard multi-Gaussian variables  $Y^{MG}$ .
2. Calculate a sphering matrix  $S^{-1/2}$  for multi-Gaussian factors:

$$S^{-1/2} = Q\Lambda^{-1/2}Q^T, \quad (4)$$

where  $Q$  is an eigenvector matrix and  $\Lambda$  is the corresponding diagonal matrix.

3. Compute an eigenvector matrix  $Q_h$  from the spectral decomposition of the cross-variogram matrix at lag  $h$ .
4. Multiply the multi-Gaussian factors by the sphering and eigenvector matrices

$$Y^{MAF} = S^{-1/2}Q_hY^{MG}. \quad (5)$$

The resulting factors will also be spatially independent. Back transformation is performed by using transposed sphering and eigenvector matrices. A combination of MAF with MGT has been applied in various geostatistical case studies (Hosseini and Asghari 2019; Erten and Deutsch 2021; Tolosana-Delgado and Mueller 2021). However, MAF is applied on a single non-zero lag distance, so its spatial decorrelation is not perfect at all lags.

### 2.3 Metrics for Comparison

In this study, RBIGP, RBIGI, PPMT and FA were compared using six metrics: multivariate normality, spatial decorrelation, execution times, qualitative assessment of the reproduction of multivariate distributions, and histogram and variogram validation. Multivariate normality (MVN) can be evaluated using different multivariate normality tests from the MVN R package (Korkmaz et al. 2014). The MVN tests in this package include Mardia's measures of multivariate skewness and kurtosis (Mardia 1970), Royston's techniques for assessing multivariate normality (Royston 1983), the Henze–Zirkler invariant consistent tests for multivariate normality (Henze and Zirkler 1990) and Energy statistics (Székely and Rizzo 2013). Many studies in geostatistics have used MVN tests to assess the performance of MGT e.g., van den Boogaart et al. (2017), Tolosana-Delgado et al. (2019) and Tolosana-Delgado and Mueller (2021). In this study, only Henze–Zirkler's and Energy tests were used based on their consistency and robustness, confirmed in some comparison and review articles (Joensuu and Vogel 2014; Ebner and Henze 2020).

A common problem with MGT methods is that they cannot ensure spatial decorrelation. In a geostatistical context, spatial decorrelation is sometimes more crucial than multivariate normality. It is, therefore, important to assess spatial decorrelation even after applying MAF. For this purpose, the quality of the spatial decorrelation was evaluated through experimental cross-variograms. In addition, a quantitative assessment of spatial decorrelation was conducted using the relative deviation from diagonality  $\tau(h)$  together with the spatial diagonalisation efficiency  $\kappa(h)$  measures suggested by Tercan (1999). The first measure compares the absolute sum of off-diagonal elements in the factor variogram matrix to the corresponding diagonal elements. The second

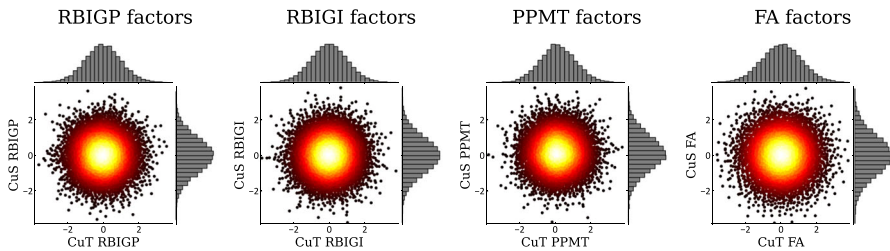


**Fig. 2** Cross plots of multi-Gaussian transformation results for case A

one compares the sum of squares of off-diagonal elements in the factor variogram matrix to the sum of squares of off-diagonal elements in the sample variogram matrix. Perfect spatial decorrelation will result in zero for  $\tau(h)$  and one for  $\kappa(h)$ .

The execution time for both forward and inverse multi-Gaussian transformations is another important factor. RBIGI, PPMT and FA were applied in a Jupyter Notebook environment, where their CPU times could be recorded. FA in the `gmGeostats` R package (Tolosana-Delgado and Mueller 2021) and the Python implementations of RBIGI and PPMT were used for the work reported in this paper. Although the original Fortran program for PPMT is much faster, the Python code may provide a fairer comparison of PPMT and RBIGI. For RBIGP, the original MATLAB code (Laparra et al. 2011) was used, in which CPU time can also be measured.

Finally, reproduction of histograms and variograms are the most critical geostatistical properties. Even though their reproduction can be assessed qualitatively, the root mean square error (RMSE) was used to obtain a quantitative comparison of results. For example, the RMSE between a hundred percentiles of original and simulated cumulative distribution functions (CDFs) were calculated for histogram validation. Similarly, RMSE measures were calculated between experimental and simulated direct and cross-variograms at multiple lag distances. Metrics such as these can be found in other geostatistical studies (Mueller and Ferreira 2012; Erten and Deutsch 2021). However, it is more difficult to provide quantitative comparisons of the reproduction of multivariate complexities, which is the primary objective of this study. For this purpose, cross-plots between simulated variables were qualitatively assessed and compared with the original plots from Fig. 1.

## 3 Results

### 3.1 Multi-Gaussian Transformation

RBIGP, RBIGI, PPMT and FA were applied to three case studies with multivariate complexities. 150 iterations were used for RBIGP, RBIGI and PPMT. For FA, input parameters were  $\sigma_0 = 0.1$  and  $\sigma_1 = 1.1$  and this method was chained twice to achieve a standard multi-Gaussian distribution. As a result, all transforms produced independent multi-Gaussian factors for total and soluble copper grades in case A (Fig. 2). RBIGI required 34 s, while PPMT and FA required 24 and 18 s, respectively.



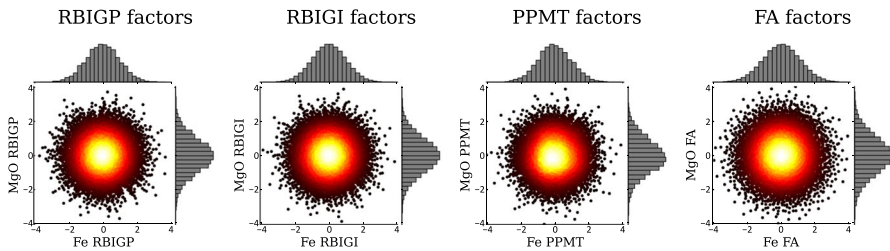


**Fig. 3** Cross plots of multi-Gaussian transformation results for case B

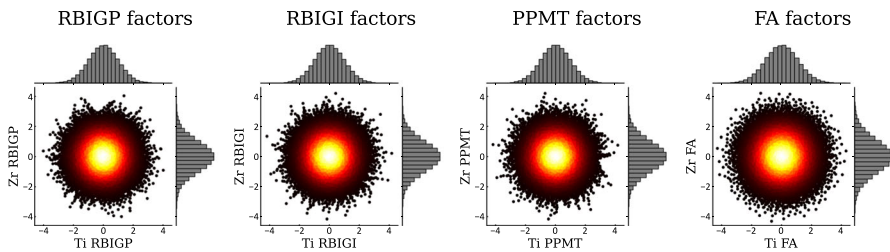


**Fig. 4** Cross plots of multi-Gaussian transformation results for case C

In case B, the non-linear relationship between iron and magnesium oxide was transformed into a multi-Gaussian distribution by all three methods (Fig. 3). However, because this case has 9,990 sample points, it took slightly more time to execute: 50 s for RBIGI, 48 s for PPMT and 51 s for FA.

Case C was more challenging to transform and Fig. 4 shows the transformed factors from all three methods. Declustering weights were not used in this case because the sum of the weights was not equal to the number of points. Furthermore, as case C comprises 33,021 titanium and zirconium samples, it takes more time to transform. For example, RBIGI and PPMT required 2 min 46 s and 2 min 42 s, respectively. On the other hand, it took FA 9 min 11 s to transform the heteroscedasticity between variables into independent factors with a multi-Gaussian distribution. In all three cases, RBIGP completed the transformation in less than one second. The significant difference in time between RBIGP and RBIGI can be explained by the different programming languages and simpler marginal Gaussianisation.

Visual inspection of kernel density estimates can assist in assessing the quality of results. However, a better way to compare the results is to check for multivariate normality. Table 2 shows the results from MVN tests applied to the transformed factors. For cases A and C, all three transforms produced multi-Gaussian distributions with perfect  $p$  values according to the Henze–Zirkler and Energy tests. PPMT, however, could not produce multi-Gaussian factors and failed both MVN tests (i.e., with  $p$  values of less than 0.05). RBIGI very slightly outperformed the other transforms based on multi-Gaussianity, particularly in cases A and B. PPMT failed to produce an MVN distribution in case B and showed slightly worse results in case A. On the other hand, all three methods produced similar results for case C. It is also important to note that

**Table 2** Multivariate normality test results for three case studies

MVN test	Case	RBIGP	RBIGI	PPMT	FA
Henze–Zirkler’s	A	0.0932 ( $p = 1$ )	0.0205 ( $p = 1$ )	0.3023 ( $p = 1$ )	0.0237 ( $p = 1$ )
	B	0.0621 ( $p = 1$ )	0.0226 ( $p = 1$ )	1.2135 ( $p < 0.05$ )	0.0270 ( $p = 1$ )
	C	0.3951 ( $p = 1$ )	0.3362 ( $p = 1$ )	0.3319 ( $p = 1$ )	0.3198 ( $p = 1$ )
Energy	A	0.0969 ( $p = 1$ )	0.0394 ( $p = 1$ )	0.2382 ( $p = 1$ )	0.0860 ( $p = 1$ )
	B	0.0845 ( $p = 1$ )	0.0337 ( $p = 1$ )	1.2746 ( $p < 0.05$ )	0.0740 ( $p = 1$ )
	C	0.2835 ( $p = 1$ )	0.2214 ( $p = 1$ )	0.2307 ( $p = 1$ )	0.2377 ( $p = 1$ )

**Table 3** Computed MAF matrices for multi-Gaussian factors in the three case studies

Case	Lag	RBIGP	RBIGI	PPMT	FA
A	75	$\begin{bmatrix} -0.90 & -0.45 \\ 0.45 & -0.90 \end{bmatrix}$	$\begin{bmatrix} -0.86 & 0.53 \\ -0.53 & -0.86 \end{bmatrix}$	$\begin{bmatrix} 0.24 & -0.98 \\ 0.98 & 0.24 \end{bmatrix}$	$\begin{bmatrix} 0.23 & -0.98 \\ 0.98 & 0.23 \end{bmatrix}$
B	15	$\begin{bmatrix} -0.20 & -0.99 \\ 0.99 & -0.20 \end{bmatrix}$	$\begin{bmatrix} -0.34 & -0.95 \\ 0.95 & -0.34 \end{bmatrix}$	$\begin{bmatrix} -0.79 & 0.64 \\ -0.64 & -0.79 \end{bmatrix}$	$\begin{bmatrix} -0.78 & 0.65 \\ -0.65 & -0.78 \end{bmatrix}$
C	15	$\begin{bmatrix} 0.47 & -0.89 \\ 0.89 & 0.47 \end{bmatrix}$	$\begin{bmatrix} -0.84 & 0.55 \\ -0.55 & -0.84 \end{bmatrix}$	$\begin{bmatrix} -0.77 & -0.66 \\ 0.66 & -0.77 \end{bmatrix}$	$\begin{bmatrix} -0.78 & -0.65 \\ 0.65 & -0.78 \end{bmatrix}$

the FA factors do not have a unit covariance matrix and have a standard deviation of 1.09 in all three cases.

### 3.2 Spatial Decorrelation

One of the limitations of the MGT approaches is that they can only assume spatial decorrelation. MGT methods always guarantee the decorrelation of variables at lag zero but not at further lags. Figure 5 (left column) shows that the omni-directional cross-variograms of the MGT factors deviate slightly from zero in all three case studies. A better spatial decorrelation was achieved by chaining RBIGP, RBIGI, PPMT and FA with MAF. A 75 m lag for case A and a 15 m lag for cases B and C were selected for the MAF transformation, and the resulting matrices are shown in Table 3. As a result, the decorrelated factors for cases B and C are more spatially independent, whereas case A did not show much improvement. Nevertheless, the resulting factors are significantly more decorrelated than the normal score variograms.

Another way to assess spatial decorrelation is by checking the relative deviation from diagonality  $\tau(h)$  and spatial diagonalisation efficiency  $\kappa(h)$  introduced by Tercan (1999). Figure 5 (middle and right columns) shows that chaining MGT with MAF improves spatial decorrelation. Even though case A does not appear to be much better, there is a clear decorrelation at lower lags up to 100m after applying MAF. It should also be noted that MGT methods alone are not sufficient to ensure decorrelation in case B. This is evident by  $\tau(h)$  and  $\kappa(h)$  not being close to zero and one, respectively. Such poor results can be explained by the normal score cross-variograms being very

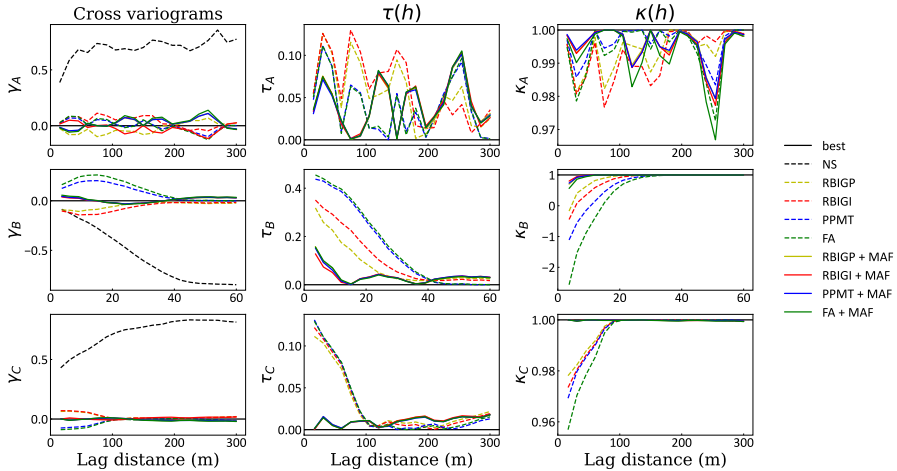


**Fig. 5** Cross-variograms, relative deviation from diagonality  $\tau(h)$  and spatial diagonalisation efficiency  $\kappa(h)$  for case A (top row), case B (middle row) and case C (bottom row) before and after applying MAF

**Table 4** Average relative deviation from diagonality  $\tau(h)$  and spatial diagonalisation efficiency  $\kappa(h)$

Method	Case A		Case B		Case C	
	$\bar{\tau}$	$\bar{\kappa}$	$\bar{\tau}$	$\bar{\kappa}$	$\bar{\tau}$	$\bar{\kappa}$
RBIGP	0.0550	0.9939	0.0825	0.8755	0.0285	0.9967
RBIGI	0.0606	0.9924	0.1106	0.8046	0.0287	0.9963
PPMT	0.0394	0.9960	0.1595	0.6562	0.0275	0.9960
FA	0.0397	0.9940	0.1662	0.4299	0.0279	0.9942
RBIGP+MAF	0.0416	0.9956	0.0364	0.9780	0.0105	0.9998
RBIGI+MAF	0.0424	0.9952	0.0338	0.9852	0.0107	0.9998
PPMT+MAF	0.0418	0.9956	0.0363	0.9805	0.0103	0.9998
FA+MAF	0.0426	0.9933	0.0364	0.9668	0.0103	0.9997

close to the factor cross-variograms. The average  $\tau(h)$  and  $\kappa(h)$  results are shown in Table 4.

### 3.3 Geostatistical Conditional Simulation

Direct variograms were automatically fitted before conditionally simulating the decorrelated variables. Various automated and semi-automated variogram fitting algorithms can be used for this purpose (Emery 2010; Desassis and Renard 2013) and are available in various commercial software packages. There was no significant directional anisotropy for case A, and omni-directional variograms were modelled for the RBIG, PPMT and FA factors (Fig. 6). The spatial variability is very similar among the three transforms, which means that any differences between generated realisations will be due mainly to the back-transformations.

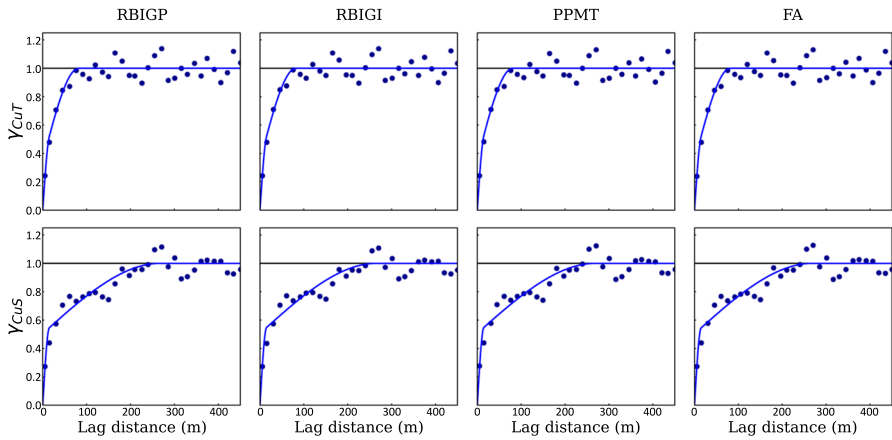


**Fig. 6** Direct variograms of decorrelated factors of total (top row) and soluble (bottom row) copper grades for case A. Experimental variograms are indicated with points and fitted theoretical variograms with solid lines

$$\begin{aligned}
 \gamma_{CuT_{RBIGP}} &= 0.342Sph(15m) + 0.658Sph(82m) \\
 \gamma_{CuS_{RBIGP}} &= 0.505Sph(15m) + 0.495Sph(267m) \\
 \gamma_{CuT_{RBIGI}} &= 0.342Sph(15m) + 0.658Sph(82m) \\
 \gamma_{CuS_{RBIGI}} &= 0.506Sph(15m) + 0.494Sph(265m) \\
 \gamma_{CuT_{PPMT}} &= 0.347Sph(15m) + 0.653Sph(81m) \\
 \gamma_{CuS_{PPMT}} &= 0.507Sph(15m) + 0.493Sph(269m) \\
 \gamma_{CuT_{FA}} &= 0.340Sph(15m) + 0.660Sph(82m) \\
 \gamma_{CuS_{FA}} &= 0.503Sph(15m) + 0.497Sph(268m)
 \end{aligned} \tag{6}$$

On the other hand, the data in case B showed significantly different variabilities in horizontal and vertical directions. Experimental variograms of decorrelated iron and magnesium oxide factors were automatically fitted as shown in Fig. 7. However, for MAF to provide a decorrelation at all lags, spatial variability must be represented by a two-structured LMC (Desbarats and Dimitrakopoulos 2000). In cases A and B, the co-regionalisation models appear to be more complex and thus experimental variograms could not be fitted to two nested structures. Nevertheless, chaining MAF and MGT still demonstrates better results, even when two-structured LMC cannot be produced (Hosseini and Asghari 2019; Erten and Deutsch 2021).

$$\begin{aligned}
 \gamma_{Fe_{RBIGP}} &= 0.380Nug + 0.620Sph(20m, 75m) \\
 \gamma_{MgO_{RBIGP}} &= 0.145Nug + 0.855Sph(33m, 222m) \\
 \gamma_{Fe_{RBIGI}} &= 0.370Nug + 0.630Sph(20m, 78m) \\
 \gamma_{MgO_{RBIGI}} &= 0.140Nug + 0.860Sph(33m, 215m) \\
 \gamma_{Fe_{PPMT}} &= 0.390Nug + 0.610Sph(21m, 81m) \\
 \gamma_{MgO_{PPMT}} &= 0.146Nug + 0.854Sph(34, 213m)
 \end{aligned}$$

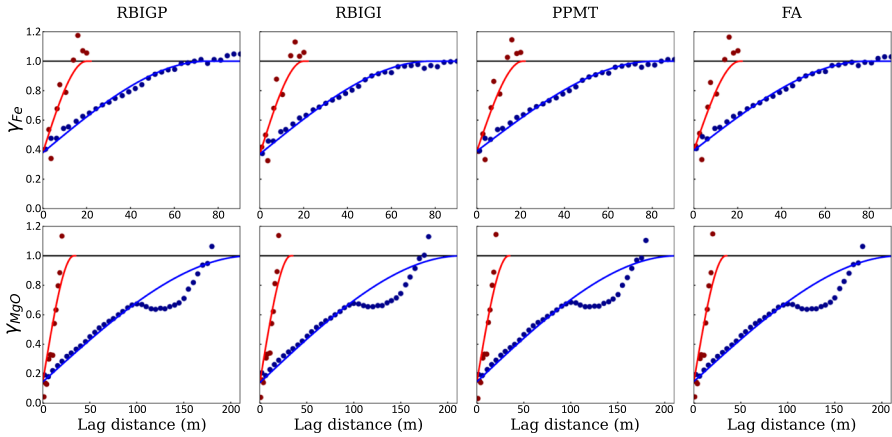


**Fig. 7** Direct variograms of decorrelated factors for iron (top row) and magnesium oxide (bottom row) for case B. Experimental variograms are indicated by points and fitted theoretical variograms by solid lines (blue: horizontal, and red: vertical)

$$\begin{aligned}
 \gamma_{Fe_{FA}} &= 0.395Nug + 0.605Sph(21m, 79m) \\
 \gamma_{MgO_{FA}} &= 0.148Nug + 0.852Sph(34m, 220m)
 \end{aligned}
 \tag{7}$$

Finally, omni-directional experimental variograms were calculated for case C. Figure 8 shows the variograms for the RBIG, PPMT and FA factors. Unlike the other two cases, variograms in case C were fitted to two nested structures.

$$\begin{aligned}
 \gamma_{Ti_{RBIGP}} &= 0.672Sph(15m) + 0.328Sph(275m) \\
 \gamma_{Z_{RBIGP}} &= 0.530Sph(15m) + 0.470Sph(275m) \\
 \gamma_{Ti_{RBIGI}} &= 0.670Sph(15m) + 0.330Sph(274m) \\
 \gamma_{Z_{RBIGI}} &= 0.531Sph(15m) + 0.469Sph(274m) \\
 \gamma_{Ti_{PPMT}} &= 0.665Sph(15m) + 0.335Sph(275m) \\
 \gamma_{Z_{PPMT}} &= 0.534Sph(15m) + 0.466Sph(275m) \\
 \gamma_{Ti_{FA}} &= 0.668Sph(15m) + 0.332Sph(275m) \\
 \gamma_{Z_{FA}} &= 0.534Sph(15m) + 0.466Sph(275m)
 \end{aligned}
 \tag{8}$$

It is evident that the factors produced by each method have almost identical spatial properties, which is true for all three cases. There were only minor differences in the variogram parameters generated by automated fitting. Using these variogram models, conditional turning bands simulation (Desassis and Renard 1973; Emery and Lantuéjoul 2006) was used to generate 50 realisations. In each case, the produced multi-Gaussian factors were modelled using identical neighbourhood parameters. Thus, most of the differences between realisations will be due to the variable transformation, which ensures a fair comparison of the MGT methods.

For case A, simulations were run on a  $61 \times 115 \times 38$  block model with grid dimension of  $30\text{ m} \times 30\text{ m} \times 10\text{ m}$ . A moving neighbourhood of  $1000\text{ m} \times 1000\text{ m} \times$

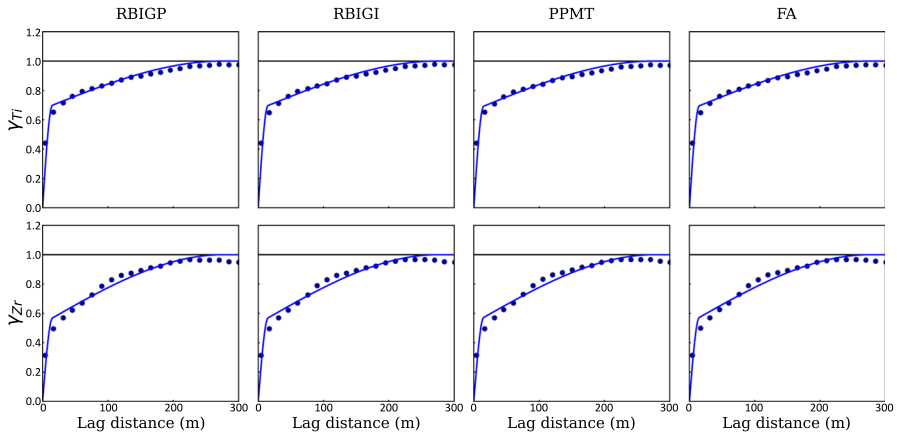


**Fig. 8** Direct variograms of decorrelated factors of titanium (top row) and zirconium (bottom row) for case C. Experimental variograms are indicated by points and the fitted theoretical variograms by solid lines

1000 m with 8 octants and 8 points per octant was used for turning bands simulation. The block model in case B consists of  $64 \times 69 \times 39$  grids with  $3 \text{ m} \times 3 \text{ m} \times 2 \text{ m}$  size, for which a  $200 \text{ m} \times 200 \text{ m} \times 200 \text{ m}$  moving neighbourhood with 8 octants and 16 points per octant was used. Finally, realisations for case C were produced on a  $65 \times 36 \times 54$  block model with a  $15 \text{ m} \times 15 \text{ m} \times 15 \text{ m}$  grid size. A  $450 \text{ m} \times 450 \text{ m} \times 450 \text{ m}$  moving neighbourhood was used with 8 octants and 40 points per octant.

### 3.4 Analysis and Validation

The simulated realisations were back-transformed to the original scale. To do so, MGT+MAF factors were first multiplied by the transposed MAF matrices (see Table 3), Then the RBIGP, RBIGI, PPMT and FA inverse transformations were applied to the corresponding multi-Gaussian realisations. In case A, RBIGP and PPMT required only 3 s to back-transform a single realisation and RBIGI required 22 s, whereas FA took 13 min and 29 s. A similar difference was observed in case B, where FA required 14 min and 30 s, RBIGI required 13 s and both RBIGP and PPMT required 2 s to back-transform one realisation. Case C is much larger than the other two, but RBIGP, RBIGI and PPMT needed only 1, 7 and 3 s, respectively. This is because their back-transformation does not require the original data, only Gaussian tables and rotation matrices at each iteration. However, as the original data are used in the FA back transformation, it took 34 min and 59 s to back-transform a single realisation for case C.

#### 3.4.1 Reproduction of Bivariate Relationships

Figure 9 (top) shows the cross plots of the back-transformed variables from a single realisation of case A. The bivariate relationships of the simulated data are similar to those of the original distribution. Although there are some artefacts above an inequality

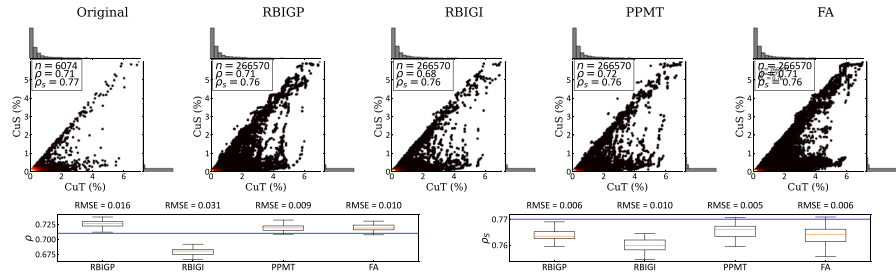


**Fig. 9** Top: cross plots of back-transformed simulated grades from one realisation compared to the original data in case A. Bottom: box plots of Pearson  $\rho$  and Spearman  $\rho_S$  correlation coefficients from 50 realisations of case A compared to the original values (solid blue lines)

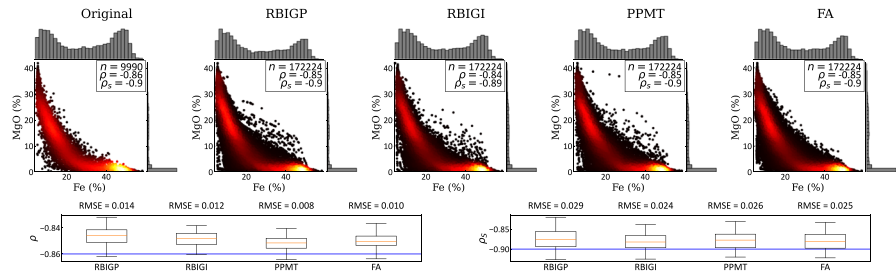


**Fig. 10** Top: cross plots of back-transformed simulated grades from one realisation compared to the original data in case B. Bottom: box plots of Pearson  $\rho$  and Spearman  $\rho_S$  correlation coefficients from 50 realisations of case B compared to the original values (solid blue lines)

constraint, this is not surprising given the skewed distributions of the copper grades. In fact, even acceptance-rejection methods that reject and re-simulate values to be within the bounds of inequality constraints do so at the cost of other statistical properties. For example, the acceptance-rejection approach performs well when marginal distributions are moderately skewed (Madani and Abulkhair 2020), but poorly reproduces other properties when dealing with very skewed distributions (Abulkhair and Madani 2021). Finally, reproduction of the Pearson and Spearman correlation coefficients suggests that PPMT performed slightly better than the others, while RBIGI underestimated the correlations (Fig. 9 bottom).

In case B, the back-transformed results show a non-linear bivariate relationship, similar to the original data (Fig. 10). Moreover, the reproduction of correlation coefficients is also almost identical.

Finally, the cross plots in Fig. 11 demonstrate that all the presented methods reproduced the heteroscedastic relationship between titanium and zirconium in case C. It can also be observed in the reproduction of the Pearson and Spearman correlation coefficients, where all three methods show similar results. However, despite similar correlations, a visual inspection suggests that FA produces better results. RBIGI produced significant outliers in the top left and bottom right corners of its cross plots in cases A and the top right corner in case C (Figs. 9, 11). On the other hand, RBIGP and

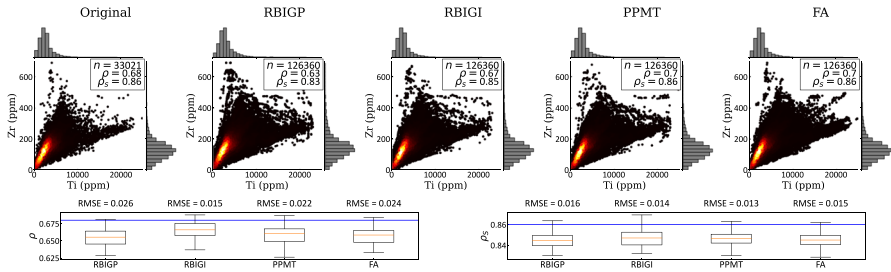


**Fig. 11** Top: cross plots of back-transformed simulated grades from one realisation compared to the original data in case C. Bottom: box plots of Pearson  $\rho$  and Spearman  $\rho_s$  correlation coefficients from 50 realisations of case B compared to the original values (solid blue lines)

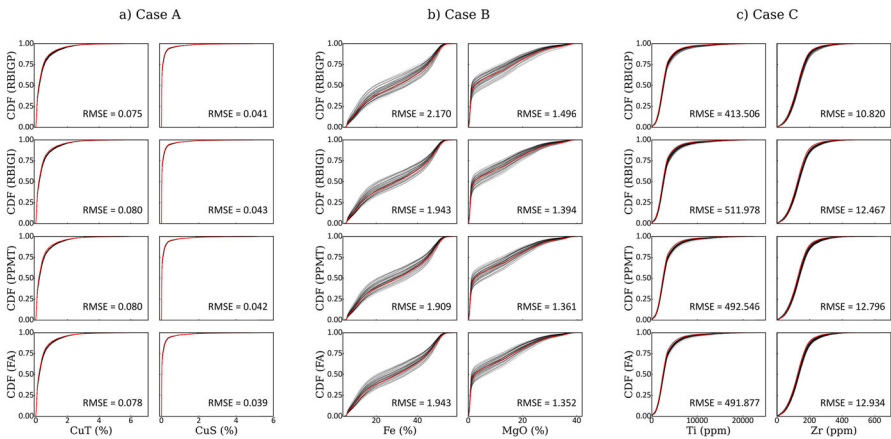


**Fig. 12** Histogram validation for case A (a), case B (b) and case C (c). The CDFs of the simulated grades are shown as solid black lines and the solid red lines are the original functions

PPMT produced minor artefacts in all three cases, which was not observed in the FA realisations.

### 3.4.2 Histogram and Variogram Validation

Histogram reproduction is another important part of geostatistical validation. Histograms of back-transformed variables of a single realisation were well reproduced in all three case studies (see Figs. 9, 10, 11). However, it is more appropriate to check all realisations, which can be accomplished by CDF or Q-Q plots. Figure 12 shows the reproduction of the CDFs of the back-transformed realisations and the RMSE values between percentiles of the realisations and the original distributions. In case A, the skewness of the distributions makes it challenging to assess and compare, but RMSE results suggest that RBIGP and FA performed slightly better than the others. Similarly, RBIGP has the least RMSE for both variables in case C, but other methods performed better in case B. Nevertheless, the difference in RMSE is insignificant, and the overall results are similar.



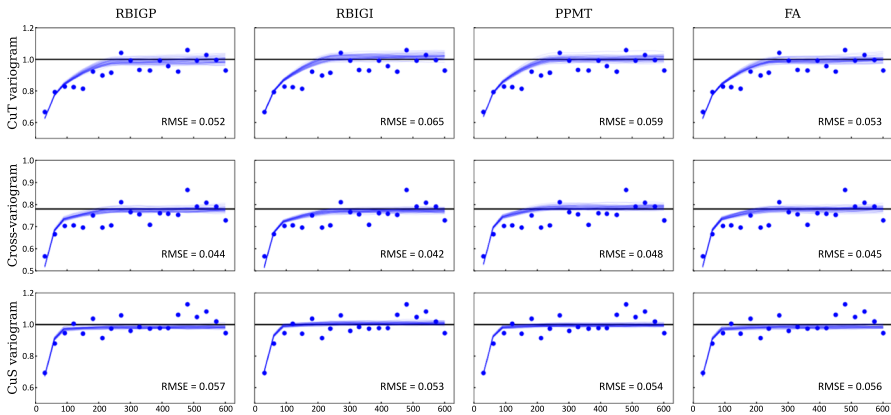


**Fig. 13** Variogram validation for case A with direct variograms in the top and bottom rows and cross-variograms in the middle row. Solid lines represent normal score variograms of simulated realisations and experimental variograms are shown as points

Reproduction of spatial variability was checked on the normal scores (i.e., first normal score transformation before iterations of RBIGP, RBIGI, PPMT and FA). The reason for this is to avoid significant deviations due to the skewness of the original variables. In addition, experimental normal score variograms were used as theoretical variograms of normal scores were not modelled. Finally, RMSE between variogram values for simulated and experimental variograms were calculated to provide a quantitative comparison of result.

Figure 13 shows the variogram validation for case A. As expected, direct variograms are well reproduced, and cross-variograms of the simulated realisations are also similar to the original points. As was observed in the histogram validation, all three methods show almost identical results from a visual standpoint. Nevertheless, it is difficult to make a comparison based on RMSE results. RBIGP and FA have smaller RMSE for total copper, but RBIGI shows better reproduction for soluble copper and cross-variability. At the same time, RBIGI also has a higher RMSE for total copper.

In case B, omni-horizontal and vertical variograms were used during the modelling due to anisotropy between those directions. Figure 14 shows the variogram validation in both the vertical and horizontal directions. Visually, the results are identical for direct and cross-variograms in both directions. However, based on RMSE, RBIGP performed the best, followed closely by other methods. There is also an underestimation of the magnesium oxide variogram for all three methods.

Finally, variogram reproduction is visually indistinguishable in case C (Fig. 15). RBIGP has a smaller RMSE for direct variograms, but the difference with other methods is insignificant. Overall, geostatistical validation metrics suggest that the performance of all four methods is similar, especially in the reproduction of marginal distributions and spatial variability. Moreover, without calculating RMSE, it is impossible to tell the difference between RBIGP, RBIGI, PPMT and FA results.

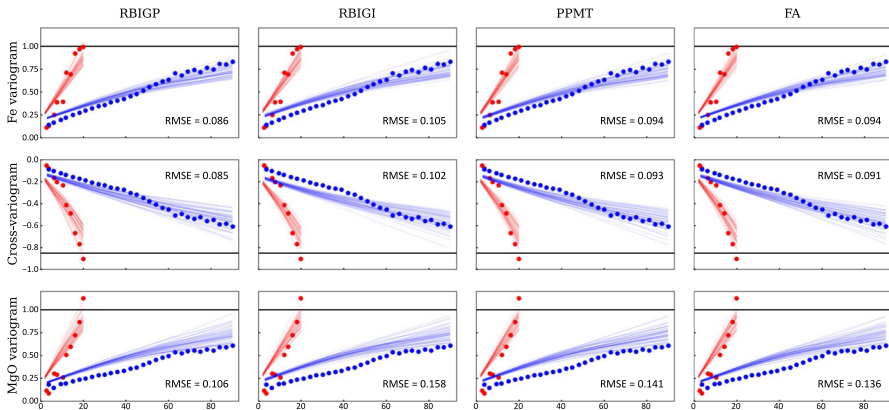


**Fig. 14** Variogram validation for case B with direct variograms in the top and bottom rows and cross-variograms in the middle. Solid lines represent normal score variograms of simulated realisations and experimental variograms are shown as points (blue: horizontal, red: vertical)

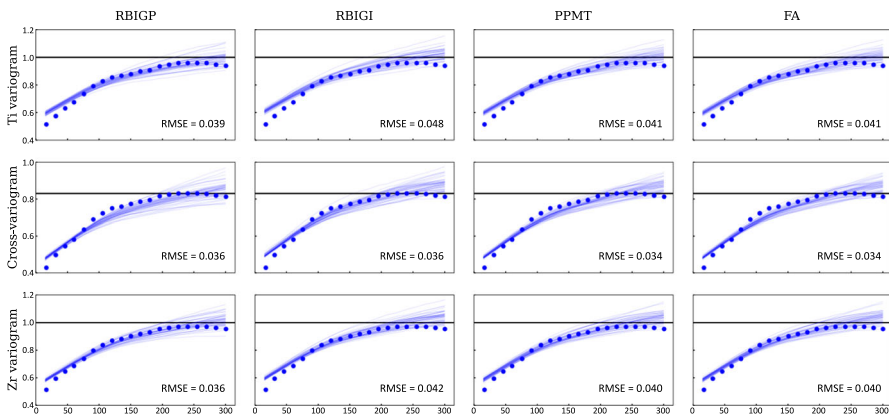


**Fig. 15** Variogram validation for case C with direct variograms in the top and bottom rows and cross-variogram in the middle row. Solid lines represent normal score variograms of simulated realisations and experimental variograms are shown as points

## 4 Discussion and Conclusions

This paper compares four MGT methods, PPMT, FA and two types of RBIG (i.e., RBIGP with PCA rotations and RBIGI with ICA rotations), using three case studies with complex multivariate relationships. All three cases were obtained from undisclosed datasets, and each represents a particular bivariate complexity with moderate-to-high correlation coefficients. Case A is a bivariate dataset with an inequality constraint between total and soluble copper grades, with 6,074 data points. It can also be called a fractional constraint since the soluble copper grade is a fraction of the total grade. Case B consists of 9990 iron and magnesium oxide samples with a non-linear relationship between them. Finally, case C has 33,021 data points, with clear heteroscedasticity between titanium and zirconium grades.

The most apparent difference between MGT approaches in this study is the execution time for forward and back transformation. Although RBIGI, PPMT and FA showed comparable times for forward transformation in cases A and B, FA took almost thrice as much time as PPMT and RBIGI in case C. Furthermore, the difference in execution time is significantly higher during the back transformation. RBIGP, RBIGI and PPMT do not need original data for the inverse transform because they save all the rotation matrices and Gaussian tables at each iteration during the fitting of transforms. Since FA requires the original data, the number of samples of the original hard data significantly affects its execution time. For example, FA required around 14 min to back-transform a single realization in cases A and B, while RBIGP, RBIGI and PPMT required only seconds. Moreover, because case C is significantly larger than the other two datasets, the time required by FA to back-transform one realisation was about 35 min. Due to a simpler and faster marginal Gaussianisation and more optimised matrix operations in MATLAB, RBIGP was significantly faster than other methods in forward transformation and similar to PPMT in inverse transformation. For example, RBIGP needed less than one second to transform the original data in all three cases.

Nevertheless, FA shows better reproduction of bivariate relationships, which was also observed by other studies reported in the geostatistical literature. PPMT has minor artefacts generated during back-transformation. While RBIGI appears to have good reproduction, it can produce significant outliers from the distribution but still within the bounds of marginals. The reason for these outliers is the convergence issue of ICA rotation, which can be unstable in some iterations. On the other hand, RBIGP does not appear to have this problem, producing results of similar quality to PPMT. Despite the minor differences, all three case studies showed that MGT methods effectively model datasets with multivariate complexities. Furthermore, all three methods show identical results in histogram and variogram validation. Even the RMSE between realisations and the original data shows no significant differences in the RBIGP, RBIGI, PPMT and FA results. Interestingly, the multivariate normality of the multi-Gaussian factors did not significantly impact the results. For example, PPMT failed MVN tests in case B but still produced realisations with a similar quality to those of other methods. However, multivariate normality plays a much bigger role in high-dimensional cases, particularly when correlations between variables are weak. Nevertheless, spatial decorrelation is much more important in geostatistical applications, and PPMT had similar spatial diagonalisation results to those of the other three methods.

Overall, the four MGT approaches analysed in this paper produce similar results in terms of multivariate normality, spatial decorrelation, reproduction of bivariate relationships, histogram and variogram validation. The main difference is the time it takes them to transform the original data and back-transform geostatistical realisations. It can be concluded that FA is not suitable for tasks requiring faster transformation, particularly when working on large datasets. For example, the recently developed rapid resource model updating methods require Gaussian transformation and must be in near real-time (Benndorf 2020). Geostatistical decorrelation methods, such as MAF and FA, were applied to rapidly update multiple cross-correlated variables (Kumar et al. 2020; Prior et al. 2021). However, we believe that RBIG and PPMT are more suitable for such tasks, especially when chained with spatial decorrelation. In future work, we

will apply RBIG and PPMT in the rapid updating of multiple variables within iron oxide copper-gold deposits.

**Acknowledgements** The research reported here was supported by the Australian Research Council Industrial Transformation Training Centre for Integrated Operations for Complex Resources (ARC ITTC IOCR—Project Number IC190100017) and funded by universities, industry and the Australian Government. The first author also acknowledges the International Association for Mathematical Geosciences for providing a Travel Grant to attend the IAMG 2022 conference and present this study. Finally, we acknowledge Geovariances for providing a demonstration version of Isatis.neo Mining Edition software.

**Author Contributions** Conceptualization: SA, PAD and CX; Methodology: SA; Investigation: SA; Writing—original draft preparation: SA; Writing—review and editing: SA, PAD and CX; Supervision: PAD and CX; Funding acquisition: PAD and CX. All authors read and approved the final manuscript.

**Funding** Open Access funding enabled and organized by CAUL and its Member Institutions.

**Code availability** Python package “*pymgt*” from ARC TC IOCR was used to perform RBIG and PPMT transformations (available at <https://github.com/exepulveda/pymgt>). FA was performed using the “*gmGeostats*” CRAN package (available at <https://cran.r-project.org/web/packages/gmGeostats>). For RBIGP, the original MATLAB code was used (available at [https://github.com/IPL-UV/rbig\\_matlab](https://github.com/IPL-UV/rbig_matlab)). MAF, variogram fitting and geostatistical modelling were performed using the Isatis.neo software.

## Declarations

**Conflict of interest** The authors declare no conflict of interest.

**Open Access** This article is licensed under a Creative Commons Attribution 4.0 International License, which permits use, sharing, adaptation, distribution and reproduction in any medium or format, as long as you give appropriate credit to the original author(s) and the source, provide a link to the Creative Commons licence, and indicate if changes were made. The images or other third party material in this article are included in the article’s Creative Commons licence, unless indicated otherwise in a credit line to the material. If material is not included in the article’s Creative Commons licence and your intended use is not permitted by statutory regulation or exceeds the permitted use, you will need to obtain permission directly from the copyright holder. To view a copy of this licence, visit <http://creativecommons.org/licenses/by/4.0/>.

## References

- Abildin Y, Madani N, Topal E (2019) A hybrid approach for joint simulation of geometallurgical variables with inequality constraint. *Minerals* 9(1):24. <https://doi.org/10.3390/min9010024>
- Abulkhair S, Madani N (2021) Assessing heterotopic searching strategy in hierarchical cosimulation for modeling the variables with inequality constraints. *C R Géosci* 353(1):115–134. <https://doi.org/10.5802/crgeos.58>
- Almeida AS, Journel AG (1994) Joint simulation of multiple variables with a Markov-type coregionalization model. *Math Geol* 26(5):565–588. <https://doi.org/10.1007/BF02089242>
- Barnett RM, Manchuk JG, Deutsch CV (2014) Projection pursuit multivariate transform. *Math Geosci* 46:337–359. <https://doi.org/10.1007/s11004-013-9497-7>
- Barnett RM, Manchuk JG, Deutsch CV (2016) The projection-pursuit multivariate transform for improved continuous variable modeling. *SPE J* 21(06):2010–2026. <https://doi.org/10.2118/184388-PA>
- Bassani MAA, Coimbra Leite Costa JF, Deutsch CV (2018) Multivariate geostatistical simulation with sum and fraction constraints. *Appl Earth Sci* 127(3):83–93. <https://doi.org/10.1080/25726838.2018.1468145>
- Benndorf J (2020) Closed loop management in mineral resource extraction. Springer, Cham

- Davis BM, Greenes KA (1983) Estimation using spatially distributed multivariate data: an example with coal quality. *J Int Assoc Math Geol* 15:287–300. <https://doi.org/10.1007/BF01036071>
- de Figueiredo LP, Schmitz T, Lunelli R, Roisenberg M, de Freitas DS, Grana D (2021) Direct multivariate simulation: a stepwise conditional transformation for multivariate geostatistical simulation. *Comput Geosci* 147(104):659. <https://doi.org/10.1016/j.cageo.2020.104659>
- Desassis N, Renard D (1973) The intrinsic random functions and their applications. *Adv Appl Probab* 5(3):439–468. <https://doi.org/10.2307/1425829>
- Desassis N, Renard D (2013) Automatic variogram modeling by iterative least squares: univariate and multivariate cases. *Math Geosci* 45:453–470. <https://doi.org/10.1007/s11004-012-9434-1>
- Desbarats A, Dimitrakopoulos R (2000) Geostatistical simulation of regionalized pore-size distributions using min/max autocorrelation factors. *Math Geol* 32:919–942. <https://doi.org/10.1023/A:1007570402430>
- Deutsch CV, Journel AG (1992) *GSLIB: geostatistical software library and user's guide*. Oxford University Press, New York
- Ebner B, Henze N (2020) Tests for multivariate normality: a critical review with emphasis on weighted  $L^2$ -statistics. *TEST* 29:845–892. <https://doi.org/10.1007/s11749-020-00740-0>
- Egozcue JJ, Pawlowsky-Glahn V, Mateu-Figueras G, Barcelo-Vidal C (2003) Reproduction of secondary data in projection pursuit transformation. *Math Geol* 35:279–300. <https://doi.org/10.1023/A:1023818214614>
- Emery X (2008) A turning bands program for conditional co-simulation of cross-correlated Gaussian random fields. *Comput Geosci* 34(12):1850–1862. <https://doi.org/10.1016/j.cageo.2007.10.007>
- Emery X (2010) Iterative algorithms for fitting a linear model of coregionalization. *Comput Geosci* 36(9):1150–1160. <https://doi.org/10.1016/j.cageo.2009.10.007>
- Emery X, Lantuéjoul C (2006) TBSIM: a computer program for conditional simulation of three-dimensional Gaussian random fields via the turning bands method. *Comput Geosci* 32(10):1615–1628. <https://doi.org/10.1016/j.cageo.2006.03.001>
- Erten O, Deutsch CV (2021) Assessment of variogram reproduction in the simulation of decorrelated factors. *Stoch Environ Res Risk Assess* 35:2583–2604. <https://doi.org/10.1007/s00477-021-02005-0>
- Friedman JH (1987) Exploratory projection pursuit. *J Am Stat Assoc* 82(397):249–266. <https://doi.org/10.1080/01621459.1987.10478427>
- Henze N, Zirkler B (1990) A class of invariant consistent tests for multivariate normality. *Commun Stat Theory Methods* 19(10):3595–3617. <https://doi.org/10.1080/03610929008830400>
- Hosseini SA, Asghari O (2015) Simulation of geometallurgical variables through stepwise conditional transformation in Sungun copper deposit, Iran. *Arab J Geosci* 8:3821–3831. <https://doi.org/10.1007/s12517-014-1452-5>
- Hosseini SA, Asghari O (2019) Multivariate geostatistical simulation on block-support in the presence of complex multivariate relationships: iron ore deposit case study. *Nat Resour Res* 28:125–144. <https://doi.org/10.1007/s11053-018-9379-2>
- Hyvarinen A (1999) Fast and robust fixed-point algorithms for independent component analysis. *IEEE Trans Neural Netw* 10(3):626–634. <https://doi.org/10.1109/72.761722>
- Joensuu DW, Vogel J (2014) A power study of goodness-of-fit tests for multivariate normality implemented in R. *J Stat Comput Simul* 84(5):1055–1078. <https://doi.org/10.1080/00949655.2012.739620>
- Journel AG (1999) Markov models for cross-covariances. *Math Geol* 31(8):955–964. <https://doi.org/10.1023/A:1007553013388>
- Journel AG, Huijbregts CJ (1978) *Mining geostatistics*. Academic Press, London
- Korkmaz S, Göksülük D, Zararsiz G (2014) MVN: an R package for assessing multivariate normality. *R Journal* 6(2):151–162
- Kumar A, Dimitrakopoulos R, Maulen M (2020) Adaptive self-learning mechanisms for updating short-term production decisions in an industrial mining complex. *J Intell Manuf* 31:1795–1811. <https://doi.org/10.1007/s10845-020-01562-5>
- Laparra V, Camps-Valls G, Malo J (2011) Iterative Gaussianization: from ICA to random rotations. *IEEE Trans Neural Networks* 22(4):537–549. <https://doi.org/10.1109/TNN.2011.2106511>
- Leuangthong O, Deutsch CV (2003) Stepwise conditional transformation for simulation of multiple variables. *Math Geol* 35(2):155–173. <https://doi.org/10.1023/A:1023235505120>
- Madani N, Abulkhair S (2020) A hierarchical cosimulation algorithm integrated with an acceptance-rejection method for the geostatistical modeling of variables with inequality constraints. *Stoch Environ Res Risk Assess* 34:1559–1589. <https://doi.org/10.1007/s00477-020-01838-5>

- Manchuk JG, Barnett RM, Deutsch CV (2017) Reproduction of secondary data in projection pursuit transformation. *Stoch Environ Res Risk Assess* 31:2585–2605. <https://doi.org/10.1007/s00477-016-1363-y>
- Mardia KV (1970) Measures of multivariate skewness and kurtosis with applications. *Biometrika* 57(3):519–530. <https://doi.org/10.1093/biomet/57.3.519>
- Mueller UA, Ferreira J (2012) The U-WEDGE transformation method for multivariate geostatistical simulation. *Math Geosci* 44:427–448. <https://doi.org/10.1007/s11004-012-9384-7>
- Mueller U, Delgado RT, Grunsky EC, McKinley JM (2020) Biplots for compositional data derived from generalized joint diagonalization methods. *Appl Comput Geosci* 8(100):044. <https://doi.org/10.1016/j.acags.2020.100044>
- Pawlowsky-Glahn V, Egozcue JJ, Tolosana-Delgado R (2015) Modeling and analysis of compositional data. Wiley, London
- Pedregosa F, Varoquaux G, Gramfort A, Michel V, Thirion B, Grisel O, Blondel M, Prettenhofer P, Weiss R, Dubourg V, Vanderplas J (2011) Scikit-learn: machine learning in Python. *J Mach Learn Res* 12:2825–2830
- Prior A, Tolosana-Delgado R, van den Boogaart KG, Benndorf J (2021) Resource model updating for compositional Geometallurgical variables. *Math Geosci* 53:945–968. <https://doi.org/10.1007/s11004-020-09874-1>
- Rossi ME, Deutsch CV (2014) Mineral resource estimation. Springer, Dordrecht
- Royston J (1983) Some techniques for assessing multivariate normality based on the Shapiro–Wilk W. *J R Stat Soc Ser C (Appl Stat)* 32(2):121–133. <https://doi.org/10.2307/2347291>
- Székely GJ, Rizzo ML (2013) Energy statistics: a class of statistics based on distances. *J Stat Plan Inference* 143(8):1249–1272. <https://doi.org/10.1016/j.jspi.2013.03.018>
- Talebi H, Mueller U, Tolosana-Delgado R, van den Boogaart KG (2019) Geostatistical simulation of geochemical compositions in the presence of multiple geological units: application to mineral resource evaluation. *Math Geosci* 51:129–153. <https://doi.org/10.1007/s11004-018-9763-9>
- Tercan AE (1999) Importance of orthogonalization algorithm in modeling conditional distributions by orthogonal transformed indicator methods. *Math Geol* 31:155–173. <https://doi.org/10.1023/A:1007557701073>
- Tercan A, Sohrabian B (2013) Multivariate geostatistical simulation of coal quality data by independent components. *Int J Coal Geol* 112:53–66. <https://doi.org/10.1016/j.coal.2012.10.007>
- Tolosana-Delgado R, Mueller U (2021) Geostatistics for compositional data with R. Springer, Cham
- Tolosana-Delgado R, Mueller U, van den Boogaart KG (2019) Geostatistics for compositional data: an overview. *Math Geosci* 51(4):485–526. <https://doi.org/10.1007/s11004-018-9769-3>
- van den Boogaart KG, Mueller U, Tolosana-Delgado R (2017) An affine equivariant multivariate normal score transform for compositional data. *Math Geosci* 49:231–251. <https://doi.org/10.1007/s11004-016-9645-y>
- Verly G (1993) Sequential Gaussian cosimulation: a simulation method integrating several types of information. In: Soares A (ed) *Geostatistics Tróia '92*. Quantitative geology and geostatistics, vol 5. Springer, Dordrecht, pp 543–554. [https://doi.org/10.1007/978-94-011-1739-5\\_42](https://doi.org/10.1007/978-94-011-1739-5_42)
- Wackernagel H (2003) Multivariate geostatistics: an introduction with applications. Springer, Berlin